ISSN 2616-5767 Vol.9, Issue 2: 87-94, DOI: 10.25236/AJETS.2026.090212

Numerical Simulation of Shot Peening for 18CrNiMo7-6 Gear Steel

Hanlin Fu[a], Haifeng Chen[b,*]

School of Mechanical and Electrical Engineering, Hunan University of Science and Technology, Xiangtan, Hunan, China
[a] fuhanlin0807@163.com, [b] chenhf1986@126.com
[*]Corresponding Author

Abstract: *Shot peening plays a key role in surface modification technique for enhancing the fatigue resistance of gear steels. This paper establishes a finite element model for multi-shot shot peening of 18CrNiMo7-6 steel based on dislocation density evolution. Using the Johnson-Cook constitutive model, Avrami coverage control, and Python random distribution methods, it systematically investigates the effects of shot diameter (0.3–0.8 mm) and velocity (30–70 m/s) on residual stresses, dislocation cell size, and dislocation density. Results indicate residual stresses exhibit a hook-shaped distribution with depth. Increasing shot diameter or velocity enhances surface dislocation density, refines dislocation cells, and shifts maximum residual compressive stress deeper into the material. Optimal parameters exist: at 60 m/s velocity, a 0.5 mm shot yields the highest surface residual compressive stress (-464.9 MPa) and maximum residual compressive stress (-745.5 MPa). Excessively large diameters (e.g., 0.8 mm) or velocities diminish strengthening effects due to uneven coverage. X-ray testing validated the model's accuracy, providing theoretical basis for process parameter optimisation.*

Keywords: *shot peening, finite element simulation, residual stress, dislocation density*

1. Introduction

As core components of mechanical transmission systems, gears directly influence equipment reliability, efficiency, and service life [1]. Under high-speed, heavy-load, and alternating load conditions, gear surfaces are prone to failure modes such as contact fatigue and fretting wear, leading to surface spalling or fracture. This severely restricts the long-term stable operation of equipment. 18CrNiMo7-6 steel, a high-performance carburising gear steel, finds extensive application in critical sectors such as aero-engine components and wind turbine gearboxes due to its excellent strength-toughness balance and carburising hardenability. However, while conventional carburising-quenching processes enhance surface hardness, the resulting residual compressive stress distribution is inadequate and exhibits steep gradients, proving ineffective in suppressing fatigue crack initiation and propagation. Shot peening technology introduces gradient nanocrystalline structures and high-density dislocations into the material surface through high-velocity shot impact, forming a residual compressive stress field with controllable depth. This makes it a key surface modification technique for enhancing gear fatigue resistance [2].

The core of the shot peening process involves accelerating shots (such as cast steel shot, glass shot, or ceramic shot) to impact the workpiece surface. Shot peening machines or guns accelerate these media using compressed air or other power sources, causing them to impact the material surface at high velocity, thereby inducing local plastic deformation and stress field changes [3]. Conventional experimental methods, constrained by testing costs and difficulties in microstructural characterisation, struggle to comprehensively reveal the influence patterns of shot peening parameters (such as peening velocity, shot diameter, and incidence angle) on residual stress field distribution, microstructural evolution, and fatigue performance. Zhang Hongwei et al. [4] examined the effect of shot size on the residual stress field in shot peening strengthening. By establishing a three-dimensional finite element model for multi-shot peening strengthening, they conducted numerical analysis. Results demonstrated that increasing shot diameter enhances the residual compressive stress layer and correspondingly increases the maximum residual compressive stress value. However, they also observed that larger shot diameter does not necessarily yield greater compressive stress values. Zhang Jinhuan et al. [5] constructed a finite element model for random shot re-shot peening. They investigated the effects of shot diameter and initial velocity on residual stress distribution, influence layer depth, and specimen surface roughness. As both shot diameter

ISSN 2616-5767 Vol.9, Issue 2: 87-94, DOI: 10.25236/AJETS.2026.090212

and initial velocity increased, residual compressive stress and influence layer depth initially rose before stabilising, while surface roughness increased. Miao et al. [6] investigated the effects of normal (90°) and oblique (60°) shot impact on target surfaces. They observed that normal impact produced higher maximum residual compressive stresses and greater surface residual compressive stresses, whereas oblique impact generated larger tensile stresses at the surface. Material microstructure and mechanical properties also undergo changes following shot peening. Experimental studies [7] revealed that shot peening refines material grain size. The finest grains typically occur at or near the surface, with grain size gradually coarsening with increasing depth. Compared to the material matrix, grain refinement significantly enhances hardness, and it is widely accepted that smaller grain size correlates with higher material strength. Analysing microstructural evolution during shot peening using numerical models has become a research focus in recent years.

To this end, this paper investigates 18CrNiMo7-6 alloy steel. Introducing a physical constitutive model based on dislocation density, a finite element model for random multi-shot shot peening is established. The objective is to systematically investigate the influence of shot diameter and peening velocity on residual stress field and dislocation cell size evolution, thereby providing theoretical foundations for optimising shot peening processes.

2. Numerical simulation methods

2.1 Shot peening finite element model

This study investigates 18CrNiMo7-6 alloy steel, employing steel wire cut shot as the shot. During simulation, as the primary focus is on the shot-peened material and the actual shot's hardness and strength significantly exceed those of the target plate, the shot is defined as a rigid body composed of carbon steel to enhance computational efficiency.

2.1.1 Target Model

In the multi-shot model, the target material dimensions are 2 × 2 × 1 mm, with the impact surface divided into three zones as illustrated in Figure 1. Zone I comprises a finely meshed region for verifying shot peening efficacy, representing the shot impact area. With a mesh size of 0.02 mm—less than one-tenth of the minimum shot diameter—this ensures the model can compute a relatively accurate residual stress distribution [8]. Zone II comprises a non-uniform mesh region, featuring coarser meshes towards the periphery and progressively finer meshes towards the centre, culminating in the same mesh size as Zone I. Given the significant plastic deformation occurring on the target surface during shot peening, both Zones I and II employ 8-node linear reduced integration elements (C3D8R). Region III comprises a single layer of infinite element mesh (CIN3D8) with a thickness of 0.2 mm to prevent stress wave reflection and oscillation. The target plate base is fully fixed within the model. The contact relationship between the shot and target plate is defined as Surface to Surface, with normal behaviour set as ‘hard’ contact and tangential behaviour as penalised friction, employing a friction coefficient of 0.3.

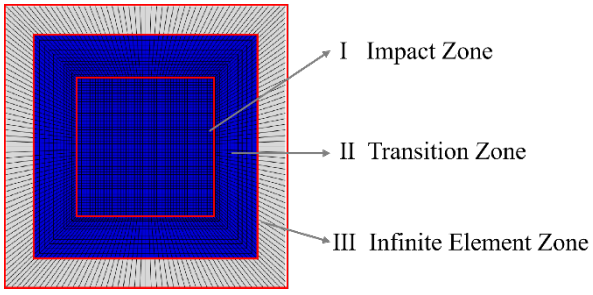

Figure 1. Target model

2.1.2 Material model

During shot peening, the surface of the material undergoes high-strain-rate plastic deformation, which leads to variations in yield stress at different strain rates. Consequently, the Johnson-Cook model [9] is employed for the plasticity parameters of 18CrNiMo7-6 material. This model is applicable to most materials undergoing high-strain-rate deformation, with yield stress expressed as:

ISSN 2616-5767 Vol.9, Issue 2: 87-94, DOI: 10.25236/AJETS.2026.090212

$$\overline{\sigma} = \left[A + B\left(\varepsilon\right)^{n} \right]\left[1 + C\ln\left(\frac{\dot{\varepsilon}}{\dot{\varepsilon}_0}\right)\right]\left(1 - \left(\frac{T - T_r}{T_m - T_r}\right)^{m} \right) \tag{1}$$

Where: $\overline{\sigma}$ is the material yield stress; A is the yield strength at the reference strain rate; B is the strain hardening coefficient; ε is the equivalent plastic strain of the material; n is the strain hardening index; C is the strain rate sensitivity coefficient; $\dot{\varepsilon}$ is the experimental strain rate; $\dot{\varepsilon}_0$ is the reference strain rate; T is the experimental temperature; T_m is the melting point of the material; T_r is the reference temperature; m is the temperature softening index. The fundamental material parameters of the sprayed target material and shot material are shown in Table 1 [10].

Table 1. Material constitutive properties and performance parameters of target materials and shot

Parameters	18CrNiMo7-6	Shots
Modulus of elasticity *E*/GPa	192	210
Poisson ratio μ	0.3	0.3
Density ρ/(g·cm^{-3})	7.85	7.85
A/MPa	338	—
B/MPa	878	—
n	0.48	—
C	0.043	—

2.2 Evolutionary Model of Dislocation Density

Estrin et al. [11] proposed a dislocation density-based constitutive model by hypothesising a grain refinement mechanism induced by plastic deformation. This model accounts for the effects of strain and strain rate on dislocation cell evolution.

The dislocation density evolution model, based on an idealised assumption of a biphasic composite microstructure in metallic materials (dislocation cell walls and dislocation cell interiors), enables the calculation of dislocation density and grain size within the plastic zone by determining the material's equivalent plastic strain and equivalent plastic strain rate. Through secondary development in ABAQUS, the equivalent plastic strain and equivalent plastic strain rate at different locations within the workpiece can be obtained at each instant during the impact process. Within the dislocation density evolution model, the total dislocation density may be regarded as the weighted sum of dislocation densities within dislocation cell walls and within dislocation cells. The growth rate of dislocation density within cells can be expressed as:

$$\Delta\rho_{\mathrm{c}} = \frac{\alpha^{*}\Delta\gamma^{\mathrm{r}}\sqrt{\rho_{\mathrm{w}}}}{\sqrt{3}b} - \frac{6\beta^{*}\Delta\gamma^{\mathrm{r}}}{bd(1-f)^{1/3}} - k_{\mathrm{c}}\Delta\gamma^{\mathrm{r}}\rho_{\mathrm{c}}\left(\frac{\Delta\gamma^{\mathrm{r}}}{\dot{\gamma}_0\Delta t}\right)^{-1/n_{\mathrm{c}}} \tag{2}$$

The growth rate of dislocation density within the cell walls can be expressed as:

$$\Delta\rho_{\mathrm{w}} = \frac{\sqrt{3}\beta^{*}\Delta\gamma^{\mathrm{r}}(1-f)\sqrt{\rho_{\mathrm{w}}}}{fb} + \frac{6\beta^{*}\Delta\gamma^{\mathrm{r}}(1-f)^{2/3}}{bdf} - k_{\mathrm{w}}\Delta\gamma^{\mathrm{r}}\rho_{\mathrm{w}}\left(\frac{\Delta\gamma^{\mathrm{r}}}{\dot{\gamma}_0\Delta t}\right)^{-1/n_{\mathrm{w}}} \tag{3}$$

Where, $\Delta\rho_{\mathrm{c}}$ and $\Delta\rho_{\mathrm{w}}$ denote the dislocation density on the dislocation cell wall and within the dislocation cell, respectively; $\dot{\gamma}_0$ is the reference resolved shear strain rate, $\Delta\gamma^{\mathrm{r}}$ is the resolved shear strain increment, α^{*}, β^{*}, k_{c} and k_{w} are material constants related to dislocation nucleation, migration, and annihilation, respectively; n_c and n_w are strain rate sensitivity coefficients, b is the magnitude of the Burgers vector, d is the grain size, f is the volume fraction of the dislocation cell walls:

$$f = f_{\infty} + (f_0 - f_{\infty})\exp\left(-\frac{\gamma^{\mathrm{r}}}{\tilde{\gamma}}\right) \tag{4}$$

Where, f_0 and f_{∞} are the initial value and saturation value of f, respectively, γ^{r} is the shear strain, and $\tilde{\gamma}$ is the decay rate of f. The total dislocation density ρ_{total} is the weighted sum of ρ_{c} and ρ_{w}, that

ISSN 2616-5767 Vol.9, Issue 2: 87-94, DOI: 10.25236/AJETS.2026.090212

is:

$$\rho_{\text{total}} = f\rho_{\text{w}} + (1-f)\rho_{\text{c}} \tag{5}$$

The relationship between the average grain size and the total dislocation density is expressed as:

$$d = \frac{K}{\sqrt{\rho_{\text{total}}}} \tag{6}$$

Where, the variable K is a parameter dependent on the accumulated plastic strain.

$$K = K_{\infty} + (K_0 - K_{\infty})\exp(-\beta\gamma^{\text{r}}) \tag{7}$$

Where, K_0 and K_{∞} are the initial state value and saturation state value of K, respectively. The constitutive model of the workpiece was implemented in the Fortran language, utilizing the VUMAT subroutine interface within ABAQUS, to integrate the constitutive model into the model and perform the calculations. Since ABAQUS cannot directly observe the evolution of dislocation cell size and dislocation density during the impact process, the dislocation cell size and dislocation density were defined as state variables “SDV22” and “SDV23”, respectively, to track their changes in the finite element post-processing interface. By feeding the equivalent plastic strain and strain rate from the current incremental step into VUMAT, the dislocation density and flow stress are updated. The dislocation cell size and dislocation density are then output as state variables SDV22 and SDV23 for post-processing inspection.

The parameters of the target material dislocation density model are shown in Table 2 [12].

Table 2. Dislocation Density Model Parameters

Parameter	α^*	β^*	k_{c}	k_{w}	n_c	n_w	f_0	f_{∞}
Value	1.05	0.097	26.15	35.95	69.09	99.54	0.25	0.06
Parameter	M	$\tilde{\gamma}$	$\rho_{\text{w}} / mm^{-2}$	$\rho_{\text{c}} / mm^{-2}$	b	$\dot{\gamma}_0 / s^{-1}$	K_0	K_{∞}
Value	3.06	3.2	5×10^{7}	2.5×10^{7}	2.5×10^{-7}	1×10^{7}	100	1

2.3 Random shot distribution and coverage control

Shot peening coverage refers to the ratio of the total area occupied by shot peening pits on the material surface to the total area of the region to be shot peened. In previous literature, the vast majority of studies altered coverage by increasing a fixed number of shot particles. This approach fails to quantitatively specify the exact numerical value of coverage. Furthermore, when the shot diameter changes, the coverage varies even if the number of particles remains constant. In prior research, an indentation area exceeding 98% of the target material's total area to be shot-peened was considered to achieve 100% coverage [13].

Through single-shot simulation, the crater diameter d for different shot sizes and the PEEQ threshold ε_p generated by shot impact on the target material can be determined, as illustrated. To calculate the required number of shots for a specific coverage rate, this paper employs the Avrami formula [14], commonly used for evaluating shot blasting coverage:

$$C = \left[1 - \exp\left(-\frac{\pi \bar{r}^{-2} n}{A}\right)\right] \times 100\% \tag{8}$$

In the formula: C denotes coverage; n represents the number of shots; A signifies the area of the shot peening zone, mm^2; $\bar{r}$ denotes the crater radius formed by a single shot impacting the target material perpendicularly, in millimetres. Utilizing the post-processing path function, the distance between the highest points of the circular crater's protrusions is selected as the crater diameter during post-processing.

The shot peening process involves the impact of numerous high-velocity shots upon the component surface, followed by the generation of a large number of irregular shot models. The creation of a random multi-shot peening model within ABAQUS's ‘Assembly’ process begins by establishing a single shot of diameter D. This is randomly generated using the Rand random number function provided by Python,

ISSN 2616-5767 Vol.9, Issue 2: 87-94, DOI: 10.25236/AJETS.2026.090212

with the resulting shot centre coordinates as follows:

$$\begin{cases} x_i = random.uniform(x_{\min},\ x_{\max}) \\ y_i = random.uniform(y_{\min},\ y_{\max}) \\ z_i = random.uniform(z_{\min},\ z_{\max}) \end{cases} \tag{9}$$

In the formula: $(x_{\min}, y_{\min}, z_{\min})$、$(x_{\max}, y_{\max}, z_{\max})$ denotes the spatial distribution range of the shot particles. To achieve a realistic simulation of the workpiece shot peening effect, the distance L between the centres of any two shot particles satisfies the following relationship:

$$L = \sqrt{\left(x_i + x_j\right)^2 + \left(y_i + y_j\right)^2 + \left(z_i + z_j\right)^2} > \mathrm{D} \tag{10}$$

In the formula: D denotes the diameter of the shot.

Define the target coverage rate based on shot peening conditions to determine the required number of shot particles N. Conduct multi-shot particle peening simulations, then calculate the coverage rate within the peening zone on the target material surface ε_p. If the coverage rate meets the target coverage rate, the peening effectiveness can be assessed; otherwise, the number of shot particles N must be adjusted until the coverage rate satisfies the requirement.

3. Test validation

3.1 Shot peening process for test specimens

The shot peening specimens were unheat-treated 18CrNiMo7-6 flat plates measuring 100 mm × 20 mm × 5 mm, as shown in Figure 2. The plates were subjected to shot peening using a vertical projection method on a shot peening machine.

Figure 2. Shot -peened test specimen

3.2 Residual Stress Measurement

The residual stress measurement apparatus comprises a PROTO LXRD X-ray stress tester, as illustrated in Figure 3. X-rays possess limited penetration capability through alloy steels, reaching only 10 μm. To measure residual stresses at various depths, the specimen surface undergoes electrolytic stripping using a Pulstec u-X360s portable electrolytic polishing machine.

Figure 3. PROTO LXRD X-ray Stress Tester

3.3 Experimental validation

To validate the shot peening finite element model, residual stress simulation values were compared with experimental data. In pneumatic shot peening machines, the shot velocity is altered by adjusting the

ISSN 2616-5767 Vol.9, Issue 2: 87-94, DOI: 10.25236/AJETS.2026.090212

air pressure. Consequently, the air pressure from the shot peening test was converted into the shot velocity within the simulation model. The shot velocity was calculated using an empirical formula, namely:

$$V = \frac{16.35 \times p}{1.53 \times m + p} + \frac{29.5 \times p}{0.598 \times d + p} + 4.83 \times p \tag{11}$$

In the equation: V denotes the shot velocity (m/s), m and d represent the shot flow rate (kg/min) and shot diameter (mm) respectively, while p is the air pressure (bar). At a shot velocity of 60 m/s, shot blasting simulations were conducted using shots of 0.4 mm, 0.6 mm, and 0.8 mm diameters. The results are shown in Figures 4(a–c).

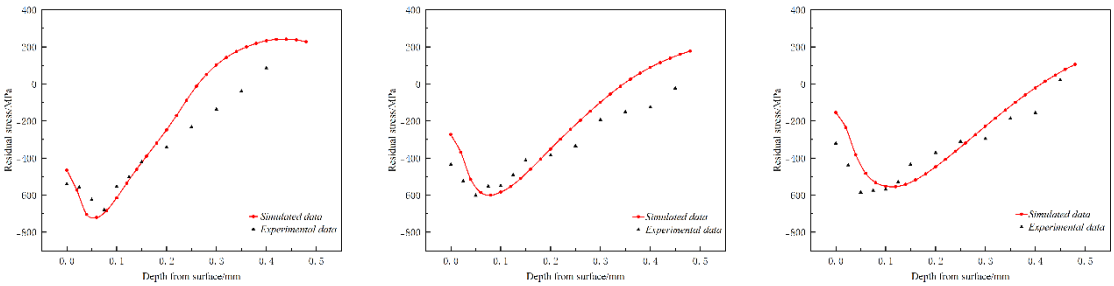

(a) (b) (c)

Figure 4. Comparison of simulated and experimental residual stress profiles for shot diameters of (a) 0.4 mm, (b) 0.6 mm, and (c) 0.8 mm at a velocity of 60 m/s.

Figures 4(a–c) present the comparison between simulated and experimental residual stress results for different shot diameters at a shot velocity of 60 m/s. Specifically, (a), (b) and (c) correspond to shot diameters of 0.4 mm, 0.6 mm and 0.8 mm respectively.

The figures demonstrate that the simulated and experimental residual stress values exhibit broadly consistent trends with depth, following a 'hook-shaped' distribution. Specifically, residual compressive stress initially increases then decreases with increasing depth. Overall, the numerical simulation results show good agreement with experimental measurements. Consequently, Figure 4 confirms that this shot peening finite element model effectively simulates the shot peening strengthening process of 18CrNiMo7-6 alloy steel.

4. Factors Affecting the Integrity of Shot-peened Surfaces

4.1 Effect of Shot Diameter

At the same shot velocity, shots of varying diameters possess distinct kinetic energies, resulting in differing residual stress distributions within the material following shot peening. Figure 5(a) presents the residual stress distribution obtained from numerical analysis of shot peening treatments on a target substrate. This analysis employed five wire-cut shot types with diameters of 0.3 mm, 0.4 mm, 0.5 mm, 0.6 mm, and 0.8 mm, conducted at a shot velocity of 60 m/s, an incidence angle of 90°, and 100% surface coverage. As the shot diameter increased from 0.3 mm to 0.5 mm, the surface residual compressive stress rose from -415.6 MPa to -464.9 MPa, while the maximum residual compressive stress increased from -598.6 MPa to -745.5 MPa. The location of the maximum residual compressive stress shifted from 60 μm to 80 μm below the surface. Concurrently, it was observed that when the shot diameter increased from 0.5 mm to 0.8 mm, both the residual compressive stress value and the maximum residual compressive stress value at the material surface decreased. This occurs because increasing the shot diameter reduces the number of shots calculated using Eq. (8). Furthermore, the random distribution of shot particles leads to areas on the target surface remaining uncovered, resulting in non-uniform residual stress distribution across the material's surface layer. Consequently, averaging the residual stresses across all surface layer nodes causes the simulated residual compressive stress value to decrease. When both shot diameter and velocity are substantial, the coverage calculation method and the randomness of shot impact locations exert a significant influence on the residual compressive stress distribution.

Changes in dislocation cell size and dislocation density for different shot diameters are shown in Figure 5 (b) and (c) respectively. As shot diameter increases, near-surface dislocation cells become finer while the depth of the dislocation cell layer gradually increases. At the same depth, dislocation density increases and dislocation cell size gradually decreases with increasing shot diameter.

ISSN 2616-5767 Vol.9, Issue 2: 87-94, DOI: 10.25236/AJETS.2026.090212

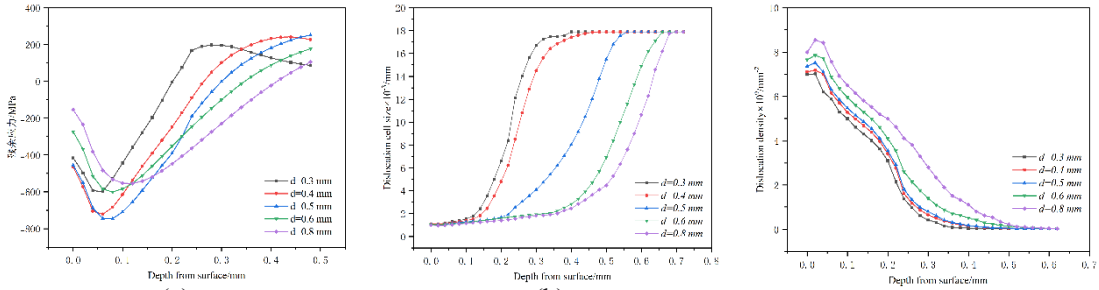

(a) (b) (c)

Figure 5. Effect of shot diameter on (a) residual stress, (b) dislocation cell size, and (c) dislocation density

4.2 Effect of Shot Velocity

At identical shot diameters, the shot velocity influences the energy imparted to the shot, resulting in distinct residual stress distributions within the material following shot peening. Figure 6(a) presents a numerical analysis of shot peening on a target material using 0.6 mm shot at a 90° incidence angle and 100% surface coverage, employing five shot velocities of 30 m/s, 40 m/s, 50 m/s, 60 m/s, and 70 m/s. This analysis yields residual stress distributions at different shot velocities. When the shot velocity increased from 30 m/s to 50 m/s, the surface residual compressive stress rose from -410.46 MPa to -449.35 MPa, while the maximum residual compressive stress increased from -574 MPa to -735.78 MPa. The location of the maximum residual compressive stress shifted from 60 μm to 80 μm below the surface. As the shot velocity continued beyond 50 m/s, the surface residual stress began to decrease. This occurred because although the energy per impact increased, the number of impacts per unit area (at constant coverage) decreased. This reduction may have led to non-uniform plastic deformation, potentially causing surface damage or microcracks, thereby relaxing part of the residual compressive stress.

Changes in dislocation cell size and dislocation density at different shot peening velocities are shown in Figures 6(b) and (c) respectively. As the shot peening velocity increases, the size of near-surface dislocation cells decreases while the depth of the dislocation cell layer gradually increases. At the same depth, dislocation density increases and dislocation cell size gradually decreases with rising shot peening velocity.

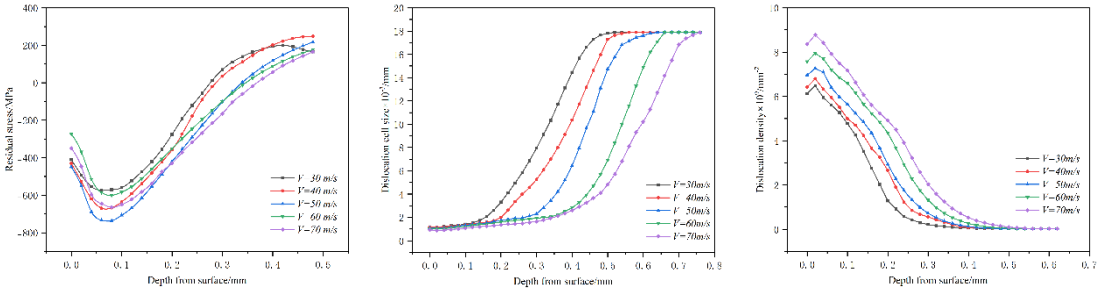

(a) (b) (c)

Figure 6. Effect of shot peening velocity on (a) residual stress ,(b) dislocation cell size, and (c) dislocation density

5. Conclusion

This study investigates the effects of shot diameter and shot velocity on residual stress fields, dislocation cell dimensions, and dislocation density in 18CrNiMo7-6 alloy steel. A finite element model based on dislocation density evolution was established for random multi-shot shot peening. Combined with experimental validation, the following key conclusions were drawn:

(1) Post-shot peening, residual stresses in the material's surface layer exhibit a ‘hook-shaped’ distribution with depth, characterised by an initial increase followed by a decrease in residual compressive stress. Both increasing shot diameter and elevating shot peening velocity significantly enhance surface dislocation density, refine dislocation cell size, and shift the location of maximum residual compressive stress to greater depths.

ISSN 2616-5767 Vol.9, Issue 2: 87-94, DOI: 10.25236/AJETS.2026.090212

(2) Shot peening parameters exert a pronounced influence on surface integrity, with an optimal parameter range identified. Under the study conditions:

At a peening velocity of 60 m/s, 0.5 mm diameter shot yielded the most favourable strengthening effect, achieving surface residual compressive stresses of -464.9 MPa and a maximum residual compressive stress of -745.5 MPa;

At an shot diameter of 0.6 mm, 50 m/s proved to be the more favorable shot peening velocity.

(3) Excessive shot peening parameters (e.g., increasing abrasive diameter to 0.8 mm) may cause uneven coverage or excessive energy input, paradoxically reducing surface residual stresses and diminishing the shot peening strengthening effect.

Acknowledgements

Project supported by the Natural Science Foundation of Hunan Province, China (Grant No. 2023JJ30241) and the Scientific Research Fund of Hunan Provincial Education Department (Grant No. 23A0375).

References

[1] Li C, Xing Z, Zhao X, et al. Research Status and Suggestions on Influence of Strengthening Methods on Bending Fatigue Strength of Heavy-duty Gear [J]. Materials Reports, 2020, 34(21): 21146-21154.
[2] Wang Z, Chen L, Zheng N, et al. A Summary of the Research on the Effect of Gear Tooth Root Strengthening on Bending Fatigue Strength based on Residual Stress [J]. Journal of Mechanical Transmission, 2019, 43(12): 161-168.
[3] Ma Y, Feng L, Xu Z, et al. Analysis on the Application and Development of Shot PeeningTechnology [J]. Modern Paint & Finishing, 2024, 27(6): 55-57.
[4] Zhang H, Zhang Y, Wu Q. Three-dimensional numerical analysis of residual stress field for shot-peening [J]. Journal of Aerospace Power, 2010, 25(3): 603-609.
[5] Zhang J, Liu H, Gan J, et al. Finite Element Simulation of Influence of Re-shot Peening Parameters on Residual Stress Evolution of Q345B Steel [J]. Materials for Mechanical Engineering, 2024, 48(8): 83-89.
[6] Miao H Y, Larose S, Perron C, et al. On the potential applications of a 3D random finite element model for the simulation of shot Peening [J]. Advances in Engineering Software, 2009, 40(10): 1023-1038.
[7] Jamalian M, Field D P. Effects of shot peening parameters on gradient microstructure and mechanical properties of TRC AZ31 [J]. Materials Characterization, 2019, 148: 9-16.
[8] Tu F, Delbergue D, Miao H, et al. A sequential DEM-FEM coupling method for shot peening Simulation [J]. Surface and Coatings Technology, 2017, 319: 200-212.
[9] Wang Z, Sun H, Wang G. Finite element analysis of effect of double shot peening on residual stress of 18CrNiMo7-6 gear steel [J]. Journal of Mechanical Transmission, 2025, 49(2): 101-110.
[10] Wu L, Lv Y, Zhang Y. Numerical simulation and experimental study of residual stress of 18CrNiMo7-6 carburized steel by ultrasonic rolling [J]. Manufacturing Technology & Machine Tool, 2023(9): 34-38, 51.
[11] Estrin Y, Tóth L S, Molinari A, et al. A Dislocation-based model for all hardening stages in large strain Deformation [J]. Acta Materialia, 1998, 46(15): 5509-5522.
[12] Lin Q, Wei P, Liu H, et al. A CFD-FEM numerical study on shot Peening[J]. International Journal of Mechanical Sciences, 2022, 223: 107259.
[13] Meo M, Vignjevic R. Finite element analysis of residual stress induced by shot peening Process [J]. Advances in Engineering Software, 2003, 34(9): 569-575.
[14] Zhao J, Tang J, Zhou W, et al. Numerical modeling and experimental verification of residual stress distribution evolution of 12Cr2Ni4A steel generated by shot Peening [J]. Surface and Coatings Technology, 2022, 430: 127993.